Available online at www.sciencedirect.com
SCIENCE DIRECT
Journal of Catalysis 235 (2005) 184–194
JOURNAL OF CATALYSIS
www.elsevier.com/locate/jcat

Selective oxidation of a pyrimidine thioether using supported tantalum catalysts

V. Cimpeanu [a], V. Pârvulescu [b], V.I. Pârvulescu [b], M. Capron [c], P. Grange [c], J.M. Thompson [d], C. Hardacre [d,*]

[a] *"C.D. Nenitzescu" Institute of Organic Chemistry, Splaiul Independentei 202B, Bucharest 060023, Romania*
[b] *Department of Chemical Technology and Catalysis, University of Bucharest, B-dul Regina Elisabeta 4-12, Bucharest 030016, Romania*
[c] *Laboratoire de Catalyse de Lille, UMR CNRS 8010, Université des Sciences et Technologies de Lille, 59 655 Villeneuve d'Ascq, France*
[d] *The QUILL Centre and School of Chemistry, Queen's University Belfast, Belfast BT9 5AG, Northern Ireland, UK*

Received 26 April 2005; revised 28 July 2005; accepted 7 August 2005

Available online 2 September 2005

Abstract

Ta_2O_5–SiO_2 catalysts were prepared by a sol–gel method using tetraethyl orthosilicate (TEOS) and tantalum (V) ethoxide as the sources of silicon and tantalum, and two families of quaternary ammonium salts, $[C_nH_{2n+1}(CH_3)_3N]Br$ ($n = 14$, 16, 18) and $[(C_nH_{2n+1})_4N]Br$ ($n = 10$, 12, 16, 18) as surfactants. The catalysts were compared for the selective sulfoxidation of 4,6-dimethyl-2-thiomethylpyrimidine using peroxide as an oxidising agent in a range of ionic liquids and organic solvents. The sol–gel catalysts were also compared with tantalum on MCM-41 prepared by grafting. The catalysts were characterized from adsorption–desorption isotherms of N_2, XRD patterns, small-angle X-ray scattering, IR spectra from adsorbed pyridine and $CDCl_3$, XPS spectra, and ^{29}Si magic angle spinning (MAS) NMR experiments. The effect of recycling on the catalyst leaching and selectivity/activity was also studied. High activities and selectivities were found in $[NTf_2]^-$ based ionic liquids and organic solvents with good recyclability of the catalyst. Tantalum was found in the solution after reaction; however, this was determined to be due to entrapment of catalyst particulates, as opposed to leaching of the active metal.

Keywords: Tantalum; 4,6-Dimethyl-2-thiomethylpyrimidine; Ionic liquid; Sulfoxidation; Heterogeneous; Mesoporous

1. Introduction

Liquid-phase selective oxidations using hydrogen peroxide with heterogeneous catalysts that are stable with respect to transition metal leaching is of significant interest to the fine and pharmaceutical chemical industries. In particular, the selective oxidation of thioethers has attracted much attention [1]. The oxidation products of these substrates are widely used as drugs, agrochemical and synthetic intermediates for valuable biologically active compounds, and synthons in the synthesis of natural products [2].

Several metals have been shown to be active and selective in such reactions, including titanium [3], molybdenum and molybdenum–antimony mixed oxides [4], and polyoxometalates [5]; however, in all of these studies, leaching of the active species into the reaction media was detected to varying degrees, with those based on titanium reportedly showing the greatest stability in molecular solvents [6]. More recently, the use of ionic liquids as alternative reaction media has been shown to significantly increase the stability of these catalysts with a wide range of structures [7–9]. Unexpectedly, the increase in the leaching stability was also accompanied by significantly greater catalytic activity.

Because of the amount of leaching seen in these studies, the heterogeneity of the catalytic process was examined, including an investigation of whether the catalysts are needed for the thioether to sulfoxide reaction. For example, Robinson et al. showed that oxidation of dialkylthioethers to the corresponding sulfoxide in the absence of a catalyst was possible, whereas oxidation to the sulfone required the use of TS-1 as the cat-

* Corresponding author.
E-mail address: c.hardacre@qub.ac.uk (C. Hardacre).

0021-9517/$ – see front matter
doi:10.1016/j.jcat.2005.08.004

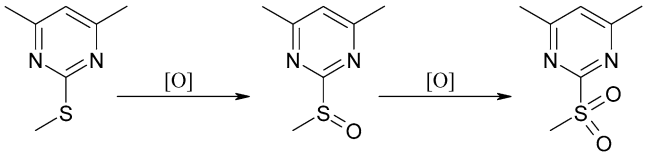

Scheme 1. Sulfoxidation of 4,6-dimethyl-2-thiomethylpyrimidine.

alyst [10]. Although homogeneous reactions were minimized using the ionic liquid, particularly in the case of Ti-SBA-15 in [emim][BF_4] [9], leaching was not totally eliminated even under these conditions, and thus the need for nonleachable active species remains important. In this regard, the present paper reports on the use of tantalum supported on silica for the selective sulfoxidation reactions in ionic liquids and organic solvents.

Meunier et al. have shown that similar catalysts with atomically dispersed tantalum are active for asymmetric epoxidation of allyl alcohols and that the catalysis was related to the surface sites and not to dissolved species [11]. This finding may not be surprising, however, because tantalum exhibits very low epoxidation activity as a dissolved species [12]. Zemski et al. reported that tantalum is an active species for the heterogeneously catalysed oxidation of *n*-butane [13]. In this case, the active site was related to tantalum oxide clusters in which the reactivity of the clusters was dependent on the composition, size, charge state, and degree of coordinative saturation. Dispersed tantalum oxide has been shown to be an effective promoter for mixed oxides in selective oxidation of propene, butanes, and xylenes [14,15], as well as in photocatalytic oxidations [16]. Recently, Wachs et al. [17] reported that increasing the size of the tantalum oxide particles to large crystallites or agglomerates reduced the oxidation capabilities of Ta due to a change in the acidic property of the clusters formed.

In the present study, highly dispersed Ta in a mesoporous-like matrix was used for the liquid phase sulfoxidation of 4,6-dimethyl-2-thiomethylpyrimidine to the corresponding sulfoxide (Scheme 1). Previous studies reported the synthesis of pure mesoporous tantalum oxide molecular sieves [18] or tantalum-silica mixed oxides organized either as silicalite molecular sieves with MFI structure [19] or as nonordered microporous–mesoporous solids [20]. The present approach examined the incorporation of dispersed tantalum oxide clusters in a nonordered monomodal and bimodal porous silica matrices using the sol–gel technique.

2. Experimental

Ta_2O_5–SiO_2 catalysts were prepared by a sol–gel method using tetraethyl orthosilicate (TEOS) and tantalum (V) ethoxide as the sources of silicon and tantalum, respectively. The silica sol was prepared from TEOS under acid hydrolysis (pH = 1.5, HCl) using a gel composition ratio of 1:4.5:50 (TEOS:H_2O:C_2H_5OH). After refluxing for 2 h at 80 °C, the solution was cooled to room temperature, and tantalum ethoxide (14 wt% in C_2H_5OH) and the surfactant were added to the sol–gel, producing a transparent gel. Gelification was carried out at room temperature. The resulting gel was dried under vacuum at 80 °C and subsequently calcined at 600 °C for 5 h. Two families of quaternary ammonium salts were used as surfactants, $[C_nH_{2n+1}(CH_3)_3N]Br$ ($n = 14$, 16, 18) and $[(C_nH_{2n+1})_4N]Br$ ($n = 10$, 12, 16, 18), with the catalysts that formed denoted as Ta-*n* and Ta-4-*n*, respectively. Tantalum on MCM-41 (Ta-MCM) was prepared using an MCM-41 support, synthesized following the procedure reported by Chen et al. [21]. Deposition of tantalum was carried out by grafting from an alcoholic solution of tantalum(V) ethoxide. All catalysts contained 15 wt% Ta_2O_5 as determined by ICP-AES.

Surface area measurements and pore size distributions were obtained from adsorption–desorption isotherms of N_2 at −196 °C using a Micromeritics ASAP 2000 apparatus after evacuation of the samples at 250 °C for 12 h. The measurements were made using both micropore and mesopore formalisms. XRD patterns were recorded with a Siemens D5000 Kristalloflex diffractometer using Cu-K_α radiation (λ = 1.5406 Å) and a 0.03° step size. Small-angle X-ray scattering (SAXS) experiments were performed with an evacuated Kratky compact camera mounted on a Siemens rotating copper anode (6 kW) with a take-off angle of 3°. Selection of Cu-K_α radiation was achieved using a Ni filter and completed by electronic discrimination. A one-dimensional proportional counter (Braun OED50M), placed at a distance of 24.5 cm from the sample, was used to record the scattering patterns. The channel width of the detector was ∼71 μm, that is, close to the resolution of the detector. Precise values of channel width and sample-to-detector distances were obtained by measuring calibration standards, namely rat-tail collagen and crystalline monodisperse oligomers with (–F–O–F–O–F–CO–) as a repeating unit, where F represents a para-linked aromatic moiety. The beam shape P(h, v) was measured in the plane of the detector in the horizontal direction (h) with 0.658 cm as the standard deviation. In the vertical direction (v), the beam was very sharp (∼300 μm FWHM), and thus was considered a delta function. The powders were measured in 1-mm-diameter Mark glass capillaries, and acquisition times of 1800 s were used throughout. The scattering of an empty capillary was also recorded, to obtain the so-called "parasitic" scattering. This parasitic scattering, scaled by sample transmittance, was subtracted from the sample scattering to obtain the parasitic-corrected scattering.

IR spectra from adsorbed pyridine and $CDCl_3$ were collected on a Bruker IFS88 infrared spectrometer. The samples were studied as self-supported discs (10–15 mg cm^{-2}) in a Pyrex IR cell with KBr windows. Before adsorption, the samples were outgassed at 450 °C under 10^{-4}–10^{-5} mbar vacuum for 4 h. The spectra were recorded after removal of the excess or weakly adsorbed pyridine at room temperature, 200 and 350 °C. In the case of deuteriated chloroform, the spectra were recorded only at room temperature after the adsorption of 100 mbar $CDCl_3$ and then again after degassing of the samples at 10^{-5} mbar.

The XPS spectra were recorded using a SSI X probe FISONS spectrometer (SSX-100/206) with monochromatic Al-K_α radiation. The spectrometer energy scale was calibrated using the Au4$f_{7/2}$ peak (binding energy, 84.0 eV). The C1s at 284.8 eV was used as an internal standard for calculating the binding energies. The peaks assigned to Ta4d, Ta4f, Si2p, and O1s levels were analyzed.

The ^{29}Si MAS NMR experiments were performed at room temperature on a Bruker ASX100 spectrometer (2.33 T) operating at a Larmor frequency of 19.89 MHz for ^{29}Si with a 4-mm probe head. The ^{29}Si MAS NMR spectra were obtained at a 5-kHz spinning rate using a single pulse excitation ($\pi/10$) with a recycle delay of 15 s to prevent saturation. The ^{29}Si chemical shifts were referenced relative to $Si(CH_3)_4$. The simulations were performed using the DMfit program [22].

1-Butyl-3-methylimidazolium triflate ([bmim][OTf]), 1-butyl-1-methyl-pyrrolidinium bis(trifluoromethanesulfonyl)amide ([bmpyr][NTf_2]), 1-butyl-3-methylimidazolium bis(trifluoromethanesulfonyl)amide ([bmim][NTf_2]), and 1-butyl-3-methylimidazolium lactate ([bmim][Lac]) were prepared in-house from the corresponding halide salts using standard literature methods [23–25]. Each ionic liquid was dried under high vacuum at 80 °C for 12 h. The purity of the ionic liquids was confirmed by ^{1}H and ^{13}C NMR spectroscopy.

Typically, the sulfoxidations were performed using 25 mg (0.16 mmol) 4,6-dimethyl-2-thiomethylpyrimidine, 5 mg catalyst, 0.2 mmol oxidant, and 0.6 g solvent stirred at 1000 rpm at 40 °C for the time required. The oxidations were performed using hydrogen peroxide as a 30 wt% solution in water (HPW), a 2 M anhydrous solution in dioxane (HPD), a 70% *tert*-butylhydroperoxide (TBHP) solution in water, or the solid urea–hydrogen peroxide complex (UHP).

Leaching and recycle tests were carried out using a double amount of catalyst (10 mg) in [bmim][OTf] after 100 min of reaction time. After the reaction was complete, the suspension was centrifuged for 5 min at 3500 rpm, the liquid phase was decanted, and the catalyst residue was washed with acetone (3×2 cm^3) to ensure that no residual ionic liquid or substrate/product remained on the catalyst. Before recycling, the catalyst was dried in air at 110 °C for 2 h. In addition, reactions were performed on the solvent after separation of the catalyst using the procedure described earlier. To assess tantalum leaching after each reaction, the tantalum content of the solvent and dried catalyst was analysed by ICP-AES. After each run, the catalysts were analysed by diffuse reflectance UV–vis (DR–UV–vis) using a UV-4 Unicam spectrophotometer equipped with an integrating sphere.

The reaction products were analysed by HPLC, ^{1}H and ^{13}C NMR spectroscopy. NMR spectra were recorded using a Bruker Avance DRX spectrometer, operating at 300 MHz for ^{1}H and 75 MHz for ^{13}C. ^{1}H NMR analysis was performed on the reaction mixture, showing very good agreement with the HPLC results. HPLC analysis was performed on an Agilent 1200 liquid chromatograph, using a C8 (Eclipse-XDC8) column with an eluent containing acetonitrile:water (1:1), at a flow rate of 1 cm^3 min^{-1}.

3. Results

3.1. Textural characterization of the catalysts

Table 1 summarises the textural characteristics of the investigated catalysts, Ta-*n*, Ta-4-*n*, and Ta-MCM. The data demonstrate that the directing agent plays an important role in defining the textural properties. Using [$C_nH_{2n+1}(CH_3)_3N$]Br ($n = 14$, 16, 18) leads to high surface area materials in which the alkyl chain length, n, had little influence on the surface area or the pore size. In contrast, the surface area and pore size of the catalysts formed using [$(C_nH_{2n+1})_4N$]Br were strongly dependent on the length of the chain. Two types of catalyst were formed using alkyl chain $n = 10$ or 12 and $n = 16$ or 18. A significant decrease in surface area was found using the longer alkyl chains, which also resulted in the formation of catalysts with a bimodal pore size distribution compared with a monomodal distribution found using alkyl chains $n = 10$ or 12. As expected, larger pore sizes were found using [$(C_nH_{2n+1})_4N$]Br compared with [$C_nH_{2n+1}(CH_3)_3N$]Br with 24-nm macropores found in Ta-4-16 and Ta-4-18.

Table 1
Textural characteristics of the investigated catalysts from N_2 adsorption–desorption isotherms at −196 °C, and SAXS

Catalyst	BET surface area (m^2 g^{-1})	Micropore area from *t*-plot surface analysis (m^2 g^{-1})	Pore size (nm)	
			N_2 adsorption	SAXS
Ta-14	724	181	3.4[a]	3.7
Ta-16	692	171	3.4[a]	3.7
Ta-18	698	178	3.6[a]	3.7
Ta-4-10	984	179	4.2[a]	3.5
Ta-4-12	832	297	4.2[a]	3.6
Ta-4-16	187	25	2.3, 24[b]	–
Ta-4-18	145	11	2.3, 24[b]	–
Ta-MCM	845	45	2.8[a]	3.1

[a] Monomodal pore size distribution.
[b] Bimodal pore size distribution.

The *t*-plot analysis of these materials indicated that in addition to mesopores, significant microporous surface area was also formed. The micropore surface areas were very similar to those determined using the micropore formalism. As found for the BET surface area, the micropore surface area of the catalysts prepared from [$C_nH_{2n+1}(CH_3)_3N$]Br was not dependent on n, whereas for [$(C_nH_{2n+1})_4N$]Br, a decrease in micropore surface area was observed with increasing values of n. The size of the micropores, as determined using the micropore formalism, was <0.8 nm for all of the catalysts.

SAXS measurements confirmed the pore size determination obtained using BET formalism. The small angle reflections ($2\theta = 2.4$–$6.1°$) indicated a two-dimensional hexagonal texture and, from the d_{100} spacing, pore sizes of 3.6 nm for Ta-14 and Ta-18 and 4.4 nm for Ta-4-10 and Ta-4-12. However, the diffraction patterns for these materials were weak, demonstrating that much of the catalyst was amorphous. This was confirmed by XRD in the wide-angle region ($2\theta = 10$–$90°$), which showed only a broad peak centred at 26.4° corresponding to the silica matrix (Fig. 1a). The absence of diffraction features associated with tantalum oxides is a good indication that the tantalum was well dispersed in the silica matrix.

In contrast, although the Ta-MCM catalyst showed BET surface area comparable to that of the Ta-*n* materials, significantly smaller micropore surface areas and pore sizes were observed. In comparison, with the parent MCM-41 material (BET surface area = 1141 m^2 g^{-1}), the deposition of tantalum led to a decrease in total surface area of >25%. The deposition of

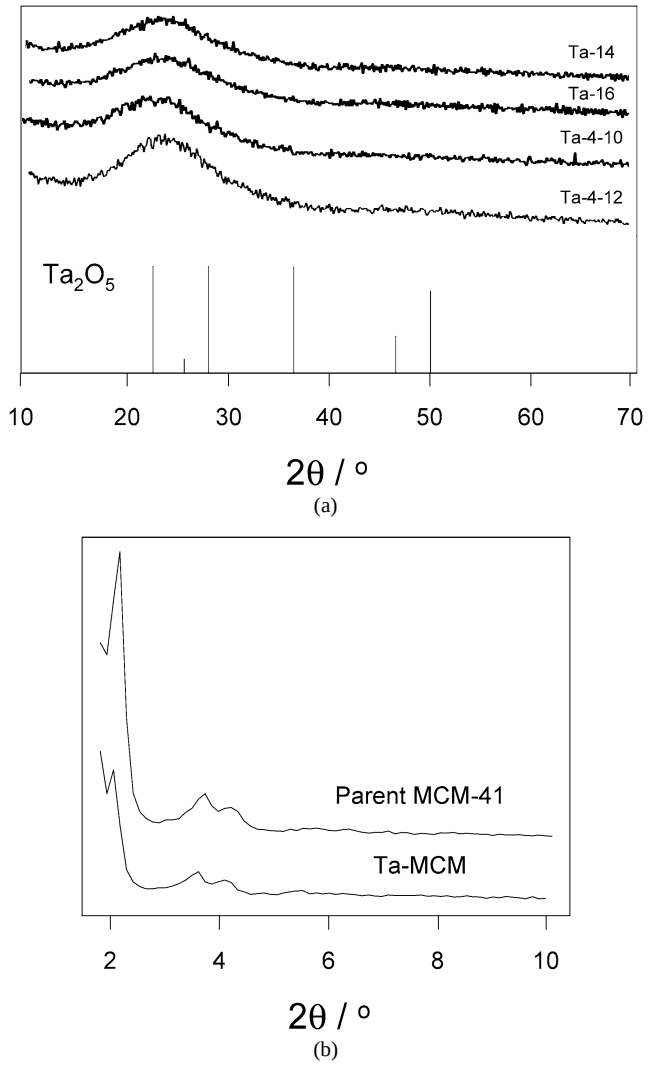

Fig. 1. XRD patterns of catalysts prepared via (a) the sol–gel method using $[C_nH_{2n+1}(CH_3)_3N]Br$ ($n = 14$, 16) and $[(C_nH_{2n+1})_4N]Br$ ($n = 10$, 12) and (b) grafting of tantalum on MCM-41 (Ta-MCM). The lines show the diffraction peak positions expected for tantalum(V) oxide.

tantalum did not affect the pore structure, with SAXS showing the well-defined 2-D hexagonal texture of MCM-41, as was expected (Fig. 1b). As found for the Ta-*n* or Ta-4-*n*, wide-angle XRD showed that no agglomeration of the tantalum oxide had occurred during the grafting onto the MCM-41 support.

3.2. XPS

XPS binding energies and comparative chemical and XPS determined atomic ratios are given in Table 2. As expected, the binding energies corresponding to Ta $4f_{7/2}$ level exhibit typical values for Ta^{5+} for Ta-*n*, Ta-4-*n*, and Ta-MCM catalysts [26]. A significant difference between the bulk and surface Ta/Si atomic ratios was found, with materials showing surface enrichment of tantalum in all cases. In addition, for both Ta-*n* and Ta-4-*n* catalysts, as the chain of the directing agent was lengthened, the surface Ta/Si ratio also increased, with those formed from $[(C_nH_{2n+1})_4N]Br$ showing significantly higher ratios than those prepared using $[C_nH_{2n+1}(CH_3)_3N]Br$. It is not clear whether the increase in the Ta/Si ratio observed is due to the decreased tantalum found in the pores of the catalyst or to the higher dispersion of tantalum over the surface, resulting in smaller Ta_2O_5 clusters. Both scenarios would result in a higher Ta/Si ratio.

Table 2
XPS binding energies of Ta4$f_{7/2}$ and Si2$p_{3/2}$ levels and comparative XPS and chemical Ta/Si atomic ratios determined by ICP-AES

Catalyst	XPS binding energy (eV)		Ta/Si atomic ratio $\times 10^3$	
	Ta4$f_{7/2}$	Si2$p_{3/2}$	Chemical analysis	XPS
Ta-14	26.4	103.2	1.15	6.4
Ta-16	26.4	103.2	1.15	6.9
Ta-18	26.5	103.2	1.15	7.5
Ta-4-10	26.4	103.2	1.15	10.2
Ta-4-12	26.5	103.2	1.15	13.4
Ta-4-16	26.4	103.2	1.15	18.8
Ta-4-18	26.4	103.2	1.15	19.4
Ta-MCM	26.5	103.4	1.15	23.4

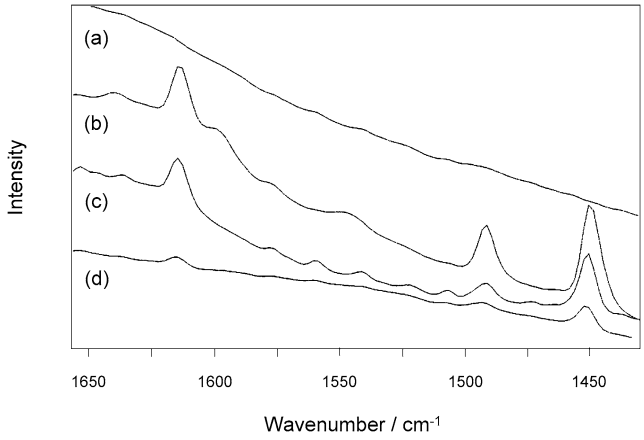

Fig. 2. IR spectra of (a) fresh Ta-14, (b) pyridine adsorption on Ta-14 at room temperature and Ta-14 following pyridine adsorption heated to (c) 200 and (d) 350 °C.

The slightly higher Ta/Si XPS atomic ratio found for Ta-MCM cannot be compared with the ratios found for the Ta-*n* or Ta-4-*n* catalysts because of the significant difference in preparation method. For example, the grafting method used in the synthesis of Ta-MCM is more likely to lead to multilayer of tantalum oxide compared with the sol–gel method.

3.3. IR spectra of adsorbed pyridine

Fig. 2 shows typical IR spectra from adsorbed pyridine (py-IR) recorded for the investigated catalysts at room temperature, 200 and 350 °C in the 1425–1650 cm^{-1} region. These spectra show typical py-IR absorption bands for solid acid materials assigned to the 8a and 19b vibration modes of adsorbed pyridine on Lewis acid sites (py-L) with bands at 1613 and 1450 cm^{-1}, and on Brønsted acid sites (py-B) with bands at 1638 and 1545 cm^{-1}. The bands at 1597, 1576, and 1490 cm^{-1} may be assigned to pyridine adsorbed on either Lewis or Brønsted acid sites [27]. Table 3 summarises how the relative intensity of the bands located at 1450 and 1545 cm^{-1} for the py-L and py-B sites, respectively, vary with temperature for the investigated

Table 3
The evolution of the relative intensity of the bands associated with pyridine adsorbed on Lewis acid sites (py-L) at 1450 cm^{-1} and pyridine adsorbed on Brønsted acid sites (py-B) at 1545 cm^{-1} at room temperature, 200 and 350 °C as a function of the catalyst

Catalyst	Intensity of py-L at 1450 cm^{-1}			Intensity of py-B at 1545 cm^{-1}		
	RT	200 °C	350 °C	RT	200 °C	350 °C
Ta-14	2.58	1.09	0.43	0.36	0	0
Ta-16	3.14	1.28	0.53	0.29	0.02	0
Ta-18	2.76	1.24	0.49	0.12	0	0
Ta-4-10	2.16	1.98	0.72	0.27	0.14	0
Ta-4-12	1.88	1.19	0.59	0.19	0	0
Ta-4-16	0.88	0.44	0.36	0	0	0
Ta-4-18	0.64	0.37	0.31	0	0	0
Ta-MCM	23.49	0.32	0.12	0	0	0

Table 4
Intensity ratios of the bands associated with the bands associated with pyridine adsorbed on Lewis acid sites (py-L) at 1450 cm^{-1} at room temperature with pyridine adsorbed on Brønsted acid sites (py-B) at 1545 cm^{-1} at room temperature and with pyridine adsorbed on Lewis acid sites (py-L) at 1450 cm^{-1} at 200 °C and 350 °C for the sol–gel-prepared and MCM catalysts

Catalyst	py-L(1450 cm^{-1})/ py-B(1545 cm^{-1}) at RT	py-L(1450 cm^{-1}, RT)/ py-L(1450 cm^{-1}, 200 °C)	py-L(1450 cm^{-1}, RT)/ py-L(1450 cm^{-1}, 350 °C)
Ta-14	7.2	2.4	6.0
Ta-16	10.8	2.4	5.9
Ta-18	23.0	2.2	5.6
Ta-4-10	8.0	1.1	3.0
Ta-4-12	9.9	1.6	3.2
Ta-4-16	–	2.0	2.4
Ta-4-18	–	1.7	2.1
Ta-MCM	–	73.4	195.7

catalysts. All of these values were normalized to the catalyst mass.

In general, the Ta-*n* catalysts showed a significantly greater number of Lewis acid sites at room temperature than the Ta-4-*n* catalysts. In addition, although the former catalysts had little systematic variation with *n*, the catalysts formed from $[(C_nH_{2n+1})_4N]Br$ showed a clear decrease in the number of Lewis acids at room temperature with increasing alkyl chain length. In contrast, the number of Brønsted acid sites decreased with increasing *n* for both sol–gel-prepared catalysts. In general, the intensity of the bands, and hence the number of acid sites, maps the surface area measurements shown in Table 1. In particular, a substantial drop in the number of acid sites was observed for the Ta-4-*n* catalysts when $n = 16$ or 18, which is consistent with the large decrease in surface area observed for those catalysts compared with $n = 10$ or 12. It is also interesting to note that the relative proportion of Lewis to Brønsted acid sites increases with chain length for both surfactants used, as shown in Table 4. For the Ta-4-*n* catalysts, where $n = 16$ or 18, the features due to the Brønsted acid sites were below the detection limit of the technique.

As expected, increasing the temperature resulted in desorption of pyridine from the surface even at 200 °C, indicating a relatively weak interaction with the acid sites. Comparing the py-L intensities at room temperature with those at 200 and 350 °C (Table 4) shows that the pyridine was bound more strongly on the Ta-4-*n* catalysts than on the Ta-*n* materials, but with no obvious trend in the strength of the pyridine adsorption as a function of *n*.

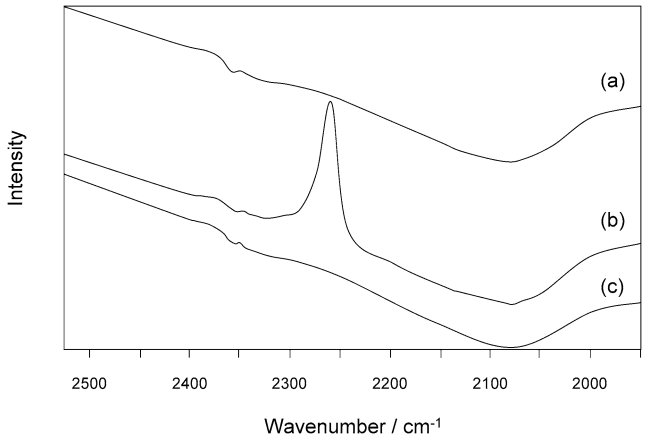

Fig. 3. IR spectra of (a) fresh Ta-14, (b) $CDCl_3$ adsorbed on Ta-14 at room temperature and (c) after outgassing following adsorption of $CDCl_3$ on Ta-14.

Table 5
Position of the $CDCl_3$-adsorption bands and the normalized intensity as a function of catalyst preparation method and directing agent used

Catalyst	Position of the $CDCl_3$ adsorption bands (cm^{-1})	Normalized intensity
Ta-14	2259	5.8
Ta-16	2259	6.1
Ta-18	2259	6.1
Ta-4-10	2262	2.5
Ta-4-12	2263	2.1
Ta-4-16	2262	0.8
Ta-4-18	2262	0.7
Ta-MCM	2262	1.1

In comparison, the sample Ta-MCM demonstrated Lewis acid sites only at room temperature and, despite a surface area similar to that of the Ta-4-*n* ($n = 10$ or 12) and Ta-*n* catalysts, a significant concentration of py-L species. However, the pyridine adsorption of Ta-MCM was much weaker than that of the sol–gel materials, as evidenced by the large desorption found at 200 and 350 °C.

For all of the catalysts studied, only weak adsorption was observed on the Brønsted acid sites. Practically no py-B bands remained after the samples were outgassed at 200 °C.

3.4. IR spectra of adsorbed $CDCl_3$

Fig. 3 shows typical IR spectra from adsorbed $CDCl_3$ for the investigated catalysts in the 2500–2000 cm^{-1} range, and Table 5 summarises the adsorption band positions and intensities normalised to the catalyst mass. The adsorption bands observed between 2263 and 2259 cm^{-1} correspond to weak basic sites and are consistent with adsorption on pure silica [28]. A small shift (~3–4 cm^{-1}) in the $CDCl_3$-adsorption bands to a lower wave number was found on comparing the Ta-*n* catalysts with the samples prepared from $[(C_nH_{2n+1})_4N]Br$ or through grafting onto MCM-41, which may indicate increased adsorp-

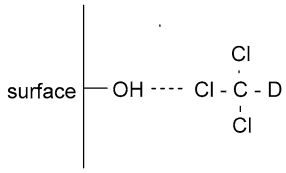

Scheme 2. Schematic of the adsorption geometry of $CDCl_3$ on the acidic catalyst surface.

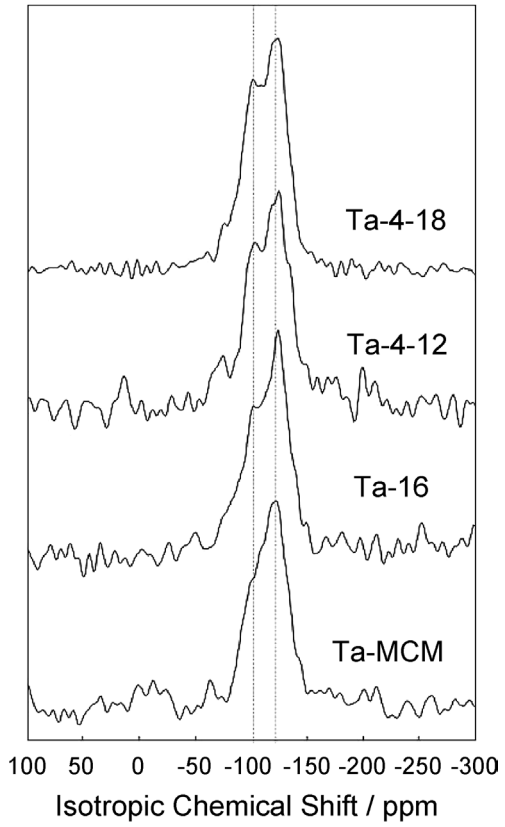

Fig. 4. ^{29}Si MAS NMR spectra of the catalysts prepared by the sol–gel route and via grafting onto MCM-41.

tion strength and thus more basic sites. In agreement with the pyridine adsorption measurements on the Lewis acid sites, the intensity of the $CDCl_3$ band was found to have little systematic variation with *n* for the Ta-*n* catalysts, whereas a decrease with *n* was observed for the Ta-4-*n* materials. However, unlike the pyridine adsorption, little $CDCl_3$ was found to bind to the Ta-MCM catalyst. The $CDCl_3$ adsorption is thought to be associated with the surface OH species, as shown in Scheme 2, and, as expected, the adsorption was accompanied by a decrease in the intensity of the band associated with the hydroxy group at 3740 cm^{-1} [29]. The weak basic strength of the surface hydroxyls is also consistent with the complete desorption of the adsorbed $CDCl_3$ on evacuation of the samples and the reappearance of the 3740 cm^{-1} hydroxy group band.

3.5. MAS NMR measurements

^{29}Si NMR spectra of Ta-MCM, Ta-16, Ta-4-12, and Ta-4-18 are shown in Fig. 4. The four catalysts signals exhibited a unique peak centred around −109 ppm that can be fitted to a minimum of five to seven components. These peaks correspond to a small variation in the local environment of the silicon atoms. The results of the simulation are given in Table 6. ^{29}Si chemical shifts in oxide systems are very sensitive to two factors, the nature of the neighbour close to the studied silicon atoms and the local environment of the silicon. These factors determine the Si–O–Si angle and Si–O bond length, with the nearest-neighbour atom type having the most influence on the isotropic chemical shift. Considering this parameter only, five different silicon environments can be conceived, denoted as Q_m, where *m* represents the number of silicon atoms in the second coordination sphere. For example, a Q_0 species can be formally written as $Si(O^-X^+)_4$, where $X \neq Si$, Q_1 is $Si(OSi)(O^-X^+)_3$, and Q_2 is $Si(OSi)_2(O^-X^+)_2$, where $0 \leqslant m \leqslant 4$ and with the isotopic chemical shift range for each value of *m* well known [30].

Table 6
Relative populations determined from the peak areas and isotropic chemical shift of the different silicon species used to model the ^{29}Si MAS NMR signals for the sol–gel- and MCM-41-supported Ta_2O_5 catalysts. The standard deviation for the chemical shift between samples was <1 ppm

Catalyst	Isotropic chemical shift (ppm)							
	Q_3				Q_4			
	89.5	95.4	100.5	103.6	106	109.3	113.8	117.5
Ta-MCM	–	7	29	5	7	37	11	4
Ta-16	4	10	30	6	–	41	9	–
Ta-4-12	13	–	41	–	4	31	11	–
Ta-4-18	4	9	35	5	8	32	7	–

Based on this, the different contributions can be separated into two main groups consisting of Q_3 species (three bridging oxygen atoms around the silicon and one nonbridging oxygen atom) at a chemical shift between −90 and −105 ppm, and Q_4 species (four bridging oxygen atoms around the silicon) at a higher chemical shift between -106 and −117 ppm. The fits using the peaks summarised in Table 6 indicate no significant differences in the relative population of the two groups for catalysts prepared by the sol–gel method, with both Ta-*n* and Ta-4-*n* materials having a summed Q_4/summed Q_3 peak area ratio of approximately 1. In contrast, the MCM-41-based material had a ratio close to 1.4, indicating that grafted catalyst had a higher degree of polymerization with less Si–O–X ($X \neq Si$) linkage. Comparing the grafting and sol–gel-prepared catalyst Q_4:Q_3 ratios suggests the existence of $(–O–Si)_3$–Ta bonds in the framework when the sol–gel process was used.

Because of the low concentration of tantalum in the catalysts, no information on the tantalum environment could be determined from the ^{181}Ta MAS NMR spectra.

3.6. DR–UV–vis spectra

DR–UV–vis spectra of the catalysts showed a significant change as a function of the reaction media used (Fig. 5). The spectra from the fresh catalysts (Ta-16 and Ta-4-16) were essentially featureless in the region associated with the tantalum oxide species band, in agreement with the high dispersion de-

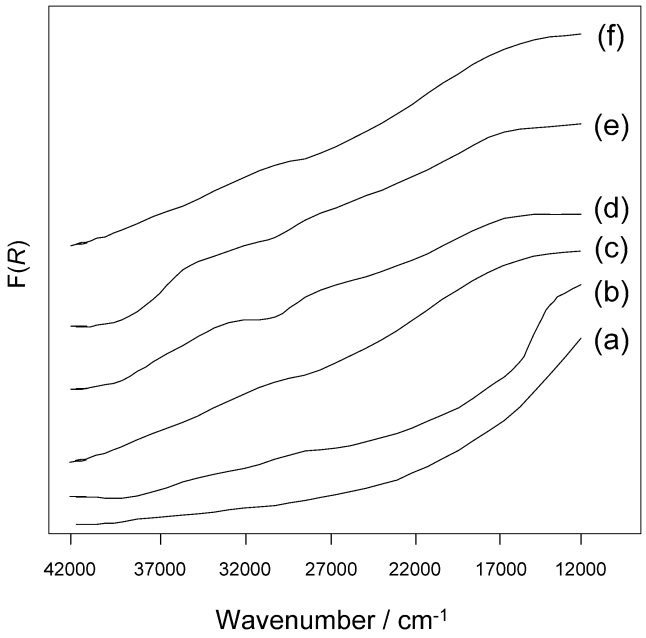

Fig. 5. DR–UV–vis spectra of (a) fresh Ta-16, (b) Ta-16 after reaction in [bmim][NTf_2], (c) fresh Ta-4-16, (d) Ta-4-16 after reaction in ethanol, (e) Ta-4-16 after reaction in dioxane and (f) Ta-4-16 after reaction in [bmim][NTf_2]. The reactions were performed using HPW for 4 h at 40 °C.

Table 7
Percentage conversion and selectivity with respect to the sulfoxide following the oxidation of 4,6-dimethyl-2-thiomethylpyrimidine using Ta-14 and HPD after 4 h at 40 °C as a function of the reaction media

Ionic liquid	Conversion (%)	Sulfoxide selectivity (%)
[bmim][NTf_2]	37.5	83.8
[bmim][OTf]	11.9	88.9
[bmim][OTf] (H^+ free)	7.7	100
[bmpyr][NTf_2]	18.7	84.2
[bmim][Lac]	0.9	100
Dioxane	34.2	81.3
Ethanol	42.7	78.2

termined for tantalum from XRD and XPS measurements. Little difference in the spectra was observed After sulfoxidation of the 4,6-dimethyl-2-thiomethyl-pyrimidine in [bmim][NTf_2], which may indicate that the dispersion of tantalum remained unchanged during the reaction. In contrast, after the reaction was performed in ethanol and dioxane, bands at ca. 36,000 and 29,300 cm^{-1} were found. The former has been reported to be due to the presence of Ta_2O_5 (36,000 cm^{-1}) [19], whereas the feature at 29,300 cm^{-1} may be due to a change in the coordination of tantalum as a consequence of exposure to oxidative conditions.

3.7. Oxidation of the 4,6-dimethyl-2-thiomethylpyrimidine

Table 7 gives the sulfoxidation yields using Ta-14 and HPD as a function of the ionic liquid and organic solvent used. Both the ionic liquid cation and anion have a significant affect on the conversion observed. As found with other sulfoxidation reactions [7], increasing the coordinating ability of the anion caused a deleterious effect, with the highest conversions found using $[NTf_2]^-$ and the least conversions found using $[Lac]^-$. It is interesting to note that almost no reaction was observed with the lactate anion, in agreement with a report of similar reactions using Ti–Ge supported on MCM-41 [7]. Therein it was proposed that the anion interacted directly with the active metal species and caused inhibition. Comparing [bmim][NTf_2] and [bmpyr][NTf_2] demonstrates a >50% decrease in the conversion, with the imidazolium cation showing higher activity than the pyrrolidinium-based ionic liquid. This again is in accordance with the previously proposed model for the Ti–Ge supported on MCM-41 catalysts. Here the cations were thought to activate the peroxy group to varying extents by increasing the electrophilicity of the oxygen. Because of the stronger hydrogen bonding capability of the imidazolium cation compared with the tetraalkylammonium species, stronger activation occurred, and increased conversion was observed. Considering the anion, it is interesting to note that the acid-free ionic liquids, prepared by metathesis from LiOTf, showed much lower rates of reaction than the corresponding ionic liquid prepared using HOTf. From previous studies, although the sulfoxidation is normally considered a Lewis acid-catalysed process, Brønsted acids may also catalyse the reaction, and the increased conversion is likely due to acid impurities from the synthesis [7]. It should be noted that with the exception of the ionic liquid prepared from HOTf, reactions performed in the absence of catalyst showed <0.5% conversion after 60 min. In the presence of 2 mM HOTf, the conversion in the ionic liquid-catalysed reaction in the absence of the heterogeneous catalyst increased to 4% after 60 min. Unlike in previous reports that used titanium-based catalysts, in which changing from conventional organic solvents to ionic liquids resulted in a significant increase in activity [7–9], similar activities were found comparing the best ionic liquid solvents with dioxane or ethanol for the tantalum systems.

High selectivities to the sulfoxide were found for all of the solvents used, with lower selectivities found in the reactions with the highest conversions, as expected. At the same conversion, only small differences in sulfoxide selectivity were observed, indicating that the solvent had little influence on the relative rates of sulfoxide and sulfone formation. No other byproducts were observed. To compare the variation with the oxidant and catalyst preparation used, all subsequent reactions were performed using [bmim][NTf_2].

Figs. 6 and 7 show the variation of the conversion and selectivity to sulfoxide using HPW and HPD as oxidants, respectively. Although similar selectivities were observed for both oxidants, a significant decrease in conversion was found using HPD compared with HPW. Both oxidants showed similar trends with respect to the variations in catalyst preparations. Varying n for the $[C_nH_{2n+1}(CH_3)_3N]Br$ surfactant had little effect on the rate of reaction, whereas a clear decrease in conversion was observed with increasing n for the $[(C_nH_{2n+1})_4N]Br$-directing agent, and almost no activity was found for Ta-4-18. Furthermore, all catalysts prepared using the sol–gel route showed lower activity than the grafted MCM-41 material. Comparing the selectivity at comparable conversions shows no clear difference between the catalysts, indicating that the nature of

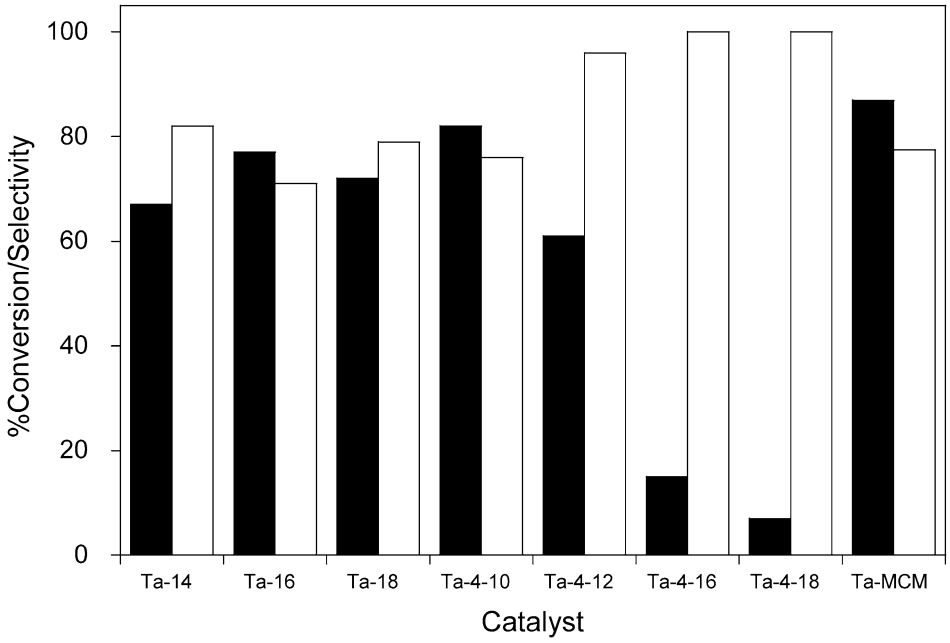

Fig. 6. Variation of the percentage conversion (■) and sulfoxide selectivity (□) for the sulfoxidation of 4,6-dimethyl-2-thiomethylpyrimidine using HPW at 40 °C over 220 min in [bmim][NTf_2] as a function of the catalyst.

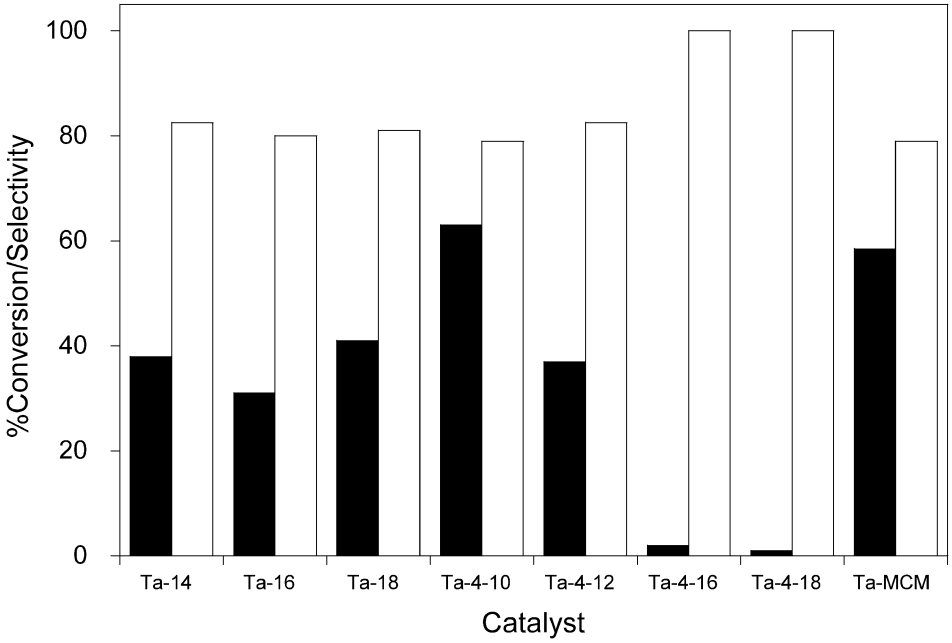

Fig. 7. Variation of the percentage conversion (■) and sulfoxide selectivity (□) for the sulfoxidation of 4,6-dimethyl-2-thiomethylpyrimidine using HPD at 40 °C over 220 min in [bmim][NTf_2] as a function of the catalyst.

the structure directing agent, its size, and the catalyst preparation method do not influence selectivity. Fig. 8 compares the conversion of 4,6-dimethyl-2-thiomethylpyrimidine using HPW, HPD, TBHP, and UHP as oxidants. Clearly, hydrogen peroxide in water was the most active oxidant of the peroxides tested, with an inverse relationship found between conversion and sulfoxide selectivity.

The variation in conversion and selectivity as a function of catalyst recycling for Ta-14, Ta-16, and Ta-MCM in [bmim][OTf] is illustrated in Fig. 9. Although a decrease in conversion, with a corresponding increase in sulfoxide selectivity, was observed for the first four reactions, thereafter the conversion remained almost unchanged for all three catalysts examined. Furthermore, using Ta-MCM, complete selectivity was achieved at 50% conversion from the fourth reaction after 100 min. Fig. 9 also shows the corresponding amount of tantalum leaching into the ionic liquid for each reaction as a function of catalyst recycling. In each case, tantalum was found

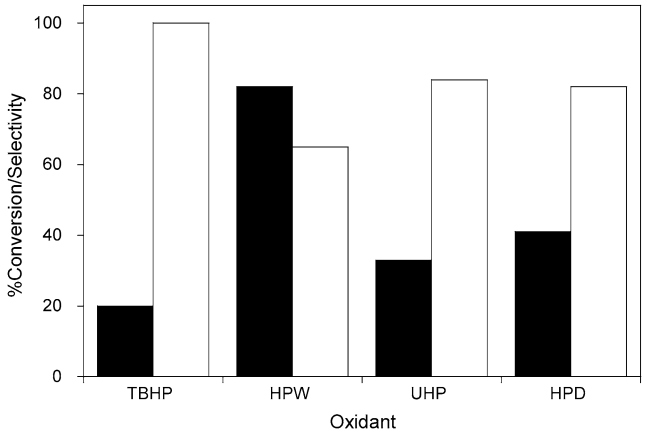

Fig. 8. Comparison of the percentage conversion (■) and sulfoxide selectivity (□) for the sulfoxidation of 4,6-dimethyl-2-thiomethylpyrimidine using Ta-14 at 40 °C over 220 min in [bmim][NTf_2] as a function of the oxidant.

in solution and, with the exception of Ta-14, the concentration decreased with increasing recyclings, eventually becoming constant at between 1 and 2%. Surprisingly, there was an increase in tantalum in the ionic liquid for Ta-14 as a function of recycling number. Similar amounts of tantalum were observed in solution on recycling using ethanol as the reaction medium; for Ta-14, 2% tantalum leaching was found over the first two reactions. Comparing the Si:Ta atomic ratio of the recycled catalyst with the fresh material reveals no significant difference in catalyst composition, indicating that the tantalum detected was due not to solvated metal, but rather to a retention of small catalyst particles in the ionic liquid on separation. This also explains how the increases and decreases in tantalum leaching depend on catalyst preparation. Increases in the Ta concentration in solution with recycling may be due to the breakup of larger aggregates as a function of stirring, and thus the "fines" will increase with reaction number, whereas the decrease can be understood by the fact that the "fines" will be gradually removed from the catalyst with each recycle. The fact that the XRD and DR–UV–vis data before and after reaction also showed little change is also consistent with this interpretation. This is in contrast with catalysts based on mesoporous titanium catalysts, where significant structural reorganisation was found after reaction, which was thought to be due to dissolution of the transition metal followed by readsorption [9]. Very low activity was found from the separated ionic liquid phase, with <20% of the activity observed in the absence of catalyst compared with that in the presence of the catalyst. Similar behaviour has been observed for vanadium- and titanium-supported silica catalysts for peroxide selective oxidation reactions by Deng et al. [31]. Therein, inseparable nanoparticles by material erosion disguised the extent to which leaching had occurred and whether or not the reaction was homogeneously catalysed. The loss in activity during recycling was also complicated by losses due to the manual manipulation; for example, 80% of the material was recovered after four reactions. Furthermore, pore blocking of the catalyst by the ionic liquid has been shown in heterogeneously catalysed hydrogenation reactions, which may also contribute to the reduction in conversion with recycling [32].

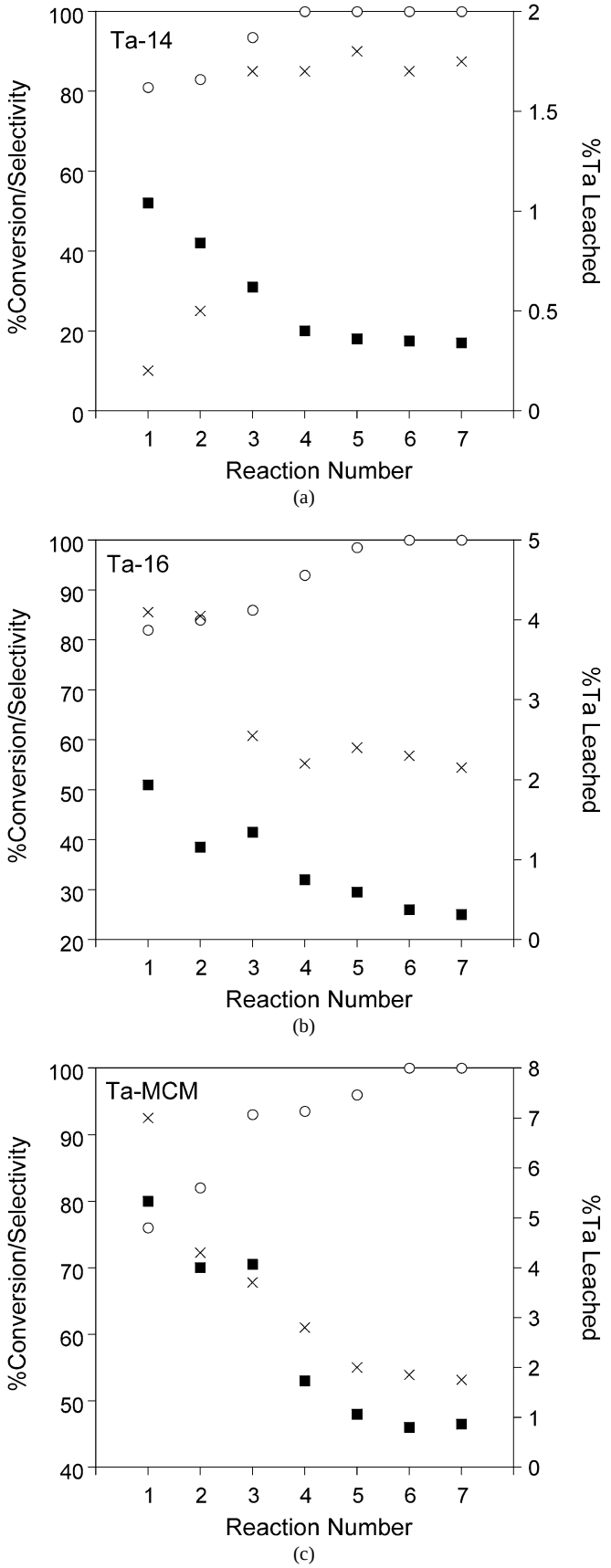

Fig. 9. Variation of the percentage conversion (■), sulfoxide selectivity (○) and Ta leached (×) as a function of recycle in [bmim][OTf] after 100 min reaction time using HPW and 10 mg of (a) Ta-14, (b) Ta-16 and (c) Ta-MCM.

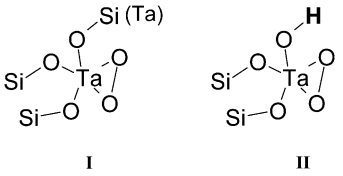

Scheme 3. Schematic of the tantalum surface species.

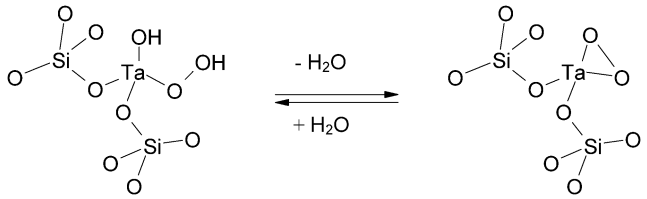

Scheme 4. Schematic of the sulfoxidation reaction site.

4. Discussion

The ^{29}Si MAS NMR and pyridine/$CDCl_3$ adsorption data demonstrate that virtually no Brønsted acid sites are present on any of the catalysts studied and that all have almost pure Lewis acid character, because no basicity was determined. This is an extremely important property of the catalyst, because it is well known that in liquid phase oxidations using hydrogen peroxide, the presence of Brønsted acidity leads to decomposition of H_2O_2, and thus a reduction in the concentration of active oxidant [33]. In the sol–gel-prepared catalysts, the local environment for the tantalum is likely to be bound via Ta–O–Si or Ta–O–Ta linkages, as shown by species **I** in Scheme 3. Because there is little evidence that the tantalum is atomically dispersed in mixed-oxide catalysts using sol–gel methods [34], a significant number of Ta–O–Ta species likely exist. Similarly, the grafting procedure on MCM-41 is likely to produce small, isolated Ta_2O_5 clusters with few Ta–O–Si bonds. In both cases, because of the lack of Brønsted acidity observed in these systems, any –OH species are likely to be terminal and not bridge-bound, that is, not Ta–O(H)–Ta/Si, as illustrated in species **II** in Scheme 3. For all of the catalysts studied, the active site is thought to be a tantalum-peroxo species.

The relative activity of the catalysts can be understood from the surface area measurements. Clearly, the rate dropped significantly as the surface area decreased, as expected. It is difficult to compare the activities for the grafted catalyst over the sol–gel-prepared material because of differences in preparation and structure of the catalysts formed. For example, comparing the rates found for the Ta-MCM catalyst with Ta-4-12 where the surface areas were similar, the conversion was increased by ∼25% for the grafted catalyst over the sol–gel-prepared material. It is likely that the difference observed is due to the higher crystallinity of the MCM catalyst, which leads to higher tantalum dispersion (hence the high Ta:Si ratio) and easier accessibility for the reactants and removal of the products.

The precise role of the directing agent in catalyst synthesis is not clear. Obviously, conventionally, the directing agent allows the formation of micelles, which are structure-determining. In this particular case, the directing agent acted as a co-solvent, influencing the orientation of the polymeric chains. Because alkoxide was introduced together with the template in an alcoholic solution, the silica gel polymerised in a controlled manner, favouring high dispersion of tantalum by avoiding rapid hydrolysis. The size/shape of the template normally controls the orientation of the polymeric chains and the hydrolysis rate; however, water was present in the synthesis mixture generating the final gel, and although some association of the template molecule occurred, this had very little effect.

It noteworthy that the excellent selectivity obtained for all of these catalysts is in agreement with the acidic character of the catalysts. The presence of Brønsted acid sites on the catalysts would easily generate an oxoanion from the hydrogen peroxide, and this species would have a more nucleophilic nature than that of structure **I** in Scheme 3 and thus would lead to overoxidation of the sulfoxide to the sulfone.

Like the reaction medium and catalyst, the hydrophilicity of the oxidant also has a strong effect on the rate of reaction, with HPW showing the greatest conversion by far. It is likely that the presence of water activates the catalyst by hydrating the Ta–O–Ta or Ta–O–Si linkages, which activates the peroxy species in a manner similar to that proposed for the hydrogen-bonding interaction of imidazolium [7] and increases the conversion (Scheme 4). This type of reaction has been observed for amorphous Ta_2O_5 in Ta-TMS-1, which readily forms superficial hydroxyl groups on contact with gas containing 0.5 Torr of water at 300 K [35]. The trend in conversion that HPW > HPD > UHP > TBHP is in line with the lack of acidity of the catalyst surface and is in agreement with the variation found with Ti-Ge-MCM-41 catalysts reported previously [7]. The low activity for the TBHP is possibly due to steric hindrance with the *tert*-butyl group, preventing strong interaction with the active site. Although this may also be true to a lesser extent for UHP, it is more likely that either the weak basicity of urea reduces the acidity of the surface, and hence the catalyst activity, or that of the urea acts as a ligand, blocking the active catalytic sites, as found in the case of coordinating anions in the ionic liquid solvents.

5. Conclusions

Both sol–gel and grafted MCM-41 catalysts with 15 wt% tantalum showed high activity and sulfoxide selectivity for the sulfoxidation of 4,6-dimethyl-2-thiomethylpyrimidine using peroxide oxidants in ionic liquids, particularly those based on the $[NTf_2]^-$ anion, as well as in dioxane and ethanol. Good recyclability was found for the catalysts, although some mechanical attrition of the catalysts was observed, which prevented total recyclability. However, this problem can be alleviated on a larger scale by directly distilling the product from the ionic liquid phase without separating the catalyst. Analysis of the catalysts postreaction indicated that the reaction was surface-catalysed. The high activity and selectivity of the catalyst were due to the lack of basic and Brønsted acid surface sites. As found for similar titanium-based catalysts, the rates of reaction were found to be strongly dependent on the cation–anion combination of the ionic liquid and the oxidant used.

Acknowledgments

This work was supported by an EU Marie Curie Early Stage Training Site Fellowship (contract HPMT-GH-00-00147-03), QUILL, and the EPSRC (grant GR/R68757).

References

[1] For example, N.M. Okun, T.M. Anderson, C.L. Hill, J. Mol. Catal. A 197 (2003) 283;
B. Notari, Stud. Surf. Sci. Catal. 37 (1988) 413;
B. Notari, Adv. Catal. 41 (1996) 253.
[2] E.N. Prilezhaeva, Russ. Chem. Rev. 69 (2000) 367;
I. Fernandez, N. Khiar, Chem. Rev. 103 (2003) 3651.
[3] R.S. Reddy, J.S. Reddy, R. Kumar, P. Kumar, J. Chem. Soc. Chem. Commun. (1992) 84;
V. Hulea, P. Moreau, F. Di Renzo, J. Mol. Catal. A 111 (1996) 325.
[4] D.C. Radu, V. Cimpeanu, F. Bertinchamps, E.M. Gaigneaux, V.I. Parvulescu, Catal. Commun. 4 (2003) 5.
[5] N.M. Okun, T.M. Anderson, C.L. Hill, J. Am. Chem. Soc. 125 (2003) 3194;
N.M. Okun, T.M. Anderson, K.I. Hardcastle, C.L. Hill, Inorg. Chem. 42 (2003) 6610.
[6] D.C. Radu, V.I. Pârvulescu, V. Cimpeanu, E. Bartha, A. Jonas, P. Grange, Appl. Catal. A 242 (2003) 77.
[7] V. Cimpeanu, V.I. Pârvulescu, P. Amorós, D. Beltrán, J.M. Thompson, C. Hardacre, Chem. Eur. J. 10 (2004) 4640.
[8] V. Cimpeanu, V.I. Pârvulescu, J.M. Thompson, C. Hardacre, Green Chem. 7 (2005) 326.
[9] V. Cimpeanu, A.N. Pârvulescu, V.I. Pârvulescu, D.T. On, S. Kaliaguine, J.M. Thompson, C. Hardacre, J. Catal. 232 (2005) 60.
[10] D.J. Robinson, L. Davies, N. McMorn, D.J. Willock, G.W. Watson, P.C.B. Page, D. Bethell, G.J. Hutchings, Phys. Chem. Chem. Phys. 2 (2000) 1523.
[11] D. Meunier, A. Piechaczyk, A. de Mallmann, J.-M. Basset, Angew. Chem. Int. Ed. 38 (1999) 3540.
[12] B.E. Rossiter, in: J.D. Morrison (Ed.), Asymmetric Synthesis, vol. 5, Academic Press, New York, 1985, p. 193.
[13] K.A. Zemski, D.R. Justes, R.C. Bell, A.W. Castleman Jr., J. Phys. Chem. A 105 (2001) 4410.
[14] Ph. Barthe, P. Macaudiere, T. Seguelong, WO Pat 96,11,740 (1996), to Rhone-Poulenc Chimie.
[15] T. Ushikubo, Catal. Today 57 (2000) 331.
[16] P.C. Roberge, S. Kaliaguine, Can. J. Chem. Eng. 60 (1982) 574;
T. Tanaka, S. Takenaka, T. Funabiki, S. Yoshida, Stud. Surf. Sci. Catal. 90 (1994) 485;
T. Tanaka, H. Nojima, T. Yamamoto, S. Takenaka, T. Funabiki, S. Yoshida, Phys. Chem. Chem. Phys. 1 (1999) 5235.
[17] Y. Chen, I.E. Wachs, J. Catal. 217 (2003) 468;
I.E. Wachs, L.E. Briand, J.-M. Jehng, L. Burcham, X. Gao, Catal. Today 57 (2000) 323.
[18] D.M. Antonelli, J.Y. Ying, Chem. Mater. 8 (1996) 874.
[19] Y.S. Ko, W.S. Ahn, Micropor. Mesopor. Mater. 30 (1999) 283.
[20] G. Guiu, P. Grange, J. Catal. 156 (1995) 132.
[21] C.-Y. Chen, H.-X. Li, M.E. Davis, Micropor. Mater. 2 (1993) 17.
[22] D. Massiot, F. Fayon, M. Capron, I. King, S. Le Calvé, B. Alonso, J.O. Durand, B. Bujoli, Z. Gan, G. Hoatson, Magn. Reson. Chem. 40 (2002) 70.
[23] P.A.Z. Suarez, J.E.L. Dullius, S. Einloft, R.F. de Souza, J. Dupont, Polyhedron 15 (1996) 1217.
[24] P. Bonhôte, A.P. Dias, N. Papageorgiou, K. Kalyanasundram, M. Grätzel, Inorg. Chem. 32 (1996) 1168.
[25] L. Cammarata, S.G. Kazarian, P.A. Salter, T. Welton, Phys. Chem. Chem. Phys. 3 (2001) 5192.
[26] S.F. Ho, S. Contarini, J.W. Rabalais, J. Phys. Chem. 91 (1987) 4779.
[27] E.E. Platero, M.P. Mentruit, C.O. Arean, A. Zecchina, J. Catal. 162 (1996) 268.
[28] E.A. Paukshtis, N.S. Kotsarenko, L.G. Karakchiev, React. Kinet. Catal. Lett. 12 (1979) 315;
E.A. Paukshtis, E.N. Yurchenko, Russ. Chem. Rev. 52 (1983) 242.
[29] H. Wiame, C. Cellier, P. Grange, J. Catal. 190 (2000) 406.
[30] G. Engelhardt, D. Michel, High Resolution Solid State NMR of Silicates and Zeolites, Wiley, New York, 1987.
[31] Y. Deng, C. Lettman, W.F. Maier, Appl. Catal. A 214 (2001) 31.
[32] K. Anderson, P. Goodrich, C. Hardacre, D.W. Rooney, Green Chem. 5 (2003) 448.
[33] D. Dumitriu, R. Bârjega, L. Frunza, D. Macovei, T. Hu, Y. Xie, V.I. Pârvulescu, S. Kaliaguine, J. Catal. 219 (2003) 337.
[34] B. Delmon, C. Sarbu, Electr. Microsc. 2 (1988) 397.
[35] J.N. Kondo, L. Lu, Y. Tahakara, K.-I. Maruya, K. Domen, N. Igarashi, T. Tatsumi, Bull. Chem. Soc. Jpn. 73 (2000) 1123.